

Article

A Semi-Analytical Model for Production Prediction of Deep CBM Wells Considering Gas-Water Two-Phase Flow

Suran Wang , Dongjun Li and Wenlan Li

CNOOC Research Institute Co., Ltd., Beijing 100028, China; lidj26@cnooc.com.cn (D.L.); liwl37@cnooc.com.cn (W.L.)

* Correspondence: wangsr@cnooc.com.cn; Tel.: +86-13551249096

Abstract: The productivity prediction of deep coalbed methane (CBM) wells is significantly influenced by gas-water two-phase flow characteristics and seepage parameters of the fracture network. While numerical simulations offer a comprehensive approach, analytical models are favored for their faster and broader applicability. However, conventional analytical models often oversimplify the complex problem of two-phase seepage equations, leading to substantial errors in dynamic analysis outcomes. Addressing this shortcoming, we establish a gas-water two-phase productivity prediction model for deep CBM reservoirs. This model takes into account the two-phase flow characteristics within the reservoir and fracture network, as well as the stress sensitivity of the reservoir and fractures. Additionally, a modified trilinear flow model characterizes the fractured modification body. By integrating the flowing material balance equation with the Newton Iteration method, we gradually update the seepage model's nonlinear parameters using the average formation pressure. We also linearize the gas-water two-phase model through successive iterations to derive a semi-analytical solution. The accuracy of the model was verified through comparison with commercial numerical simulation software results and field application. The model also enabled us to scrutinize the influence of reservoir and fracture network parameters on productivity. Our research findings suggest that the semi-analytical solution approach can efficiently address the nonlinear seepage problem of gas-water two-phase flow, enabling quick and accurate prediction of deep CBM well productivity. Moreover, appropriate fracture network parameters are paramount for enhancing the productivity of deep CBM wells. Lastly, during the development of deep CBM reservoirs, it is crucial to control the production pressure difference appropriately to minimize the stress sensitivity impact on production capacity.

Keywords: deep CBM reservoir; fractured horizontal wells; two-phase; semi-analytical model; production prediction



Citation: Wang, S.; Li, D.; Li, W. A Semi-Analytical Model for Production Prediction of Deep CBM Wells Considering Gas-Water Two-Phase Flow. *Processes* **2023**, *11*, 3022. <https://doi.org/10.3390/pr11103022>

Academic Editors: Zheng Sun, Udo Fritsching, Tao Zhang, Dong Feng, Wen Zhao and Hung Vo Thanh

Received: 17 August 2023
Revised: 7 October 2023
Accepted: 17 October 2023
Published: 20 October 2023



Copyright: © 2023 by the authors. Licensee MDPI, Basel, Switzerland. This article is an open access article distributed under the terms and conditions of the Creative Commons Attribution (CC BY) license (<https://creativecommons.org/licenses/by/4.0/>).

1. Introduction

Deep coalbed methane (CBM) reservoirs, in contrast to shallow counterparts, are typified by adverse physical properties and high in-situ stress. Consequently, conventional fracturing technologies have limited efficacy, necessitating the deployment of long horizontal wells and large-scale hydraulic fracturing technologies for their development [1–6]. CBM reservoirs, inherently comprising a dual pore media system (matrix and cleat), harbor extensive natural fractures that compound into complex networks post-fracturing [7–9]. The degree of fracturing is pivotal in defining the productivity of deep CBM wells, making the comprehension of fracturing modification imperative for the design and efficient development of deep CBM reservoirs [10–12]. Moreover, accurate prediction of deep CBM well productivity necessitates an understanding of the adsorption and desorption characteristics of deep CBM and the nonlinear flow mechanism in micro-nano pores [13–15]. CBM development invariably involves the two-phase flow stage of gas and water, the characteristics of which are notably intricate. The high in-situ stress and intense stress sensitivity of deep CBM reservoirs negatively impact gas-water seepage capacity, directly influencing

the steady productivity of gas wells [16–20]. Hence, to predict deep CBM well capacity accurately, it is crucial to consider the impact of stress sensitivity and gas-water two-phase flow characteristics. Therefore, establishing a dynamic prediction method for gas-water two-phase production in deep CBM reservoirs is paramount for deep CBM development planning, fracturing evaluation, production dynamic analysis, and prediction.

Currently, deep CBM well productivity prediction methods include analytical, semi-analytical, and numerical simulation techniques. The analytical method is typically based on steady-state seepage theory, often simplifying the equation through the introduction of the gas-water two-phase pseudo-pressure [21–25]. However, this method struggles to characterize complex seam meshes, leading to considerable errors in productivity prediction. The semi-analytical method is based on the linear flow assumption, effective in depicting the fracturing mesh modification body and expedient for calculations [26–29]. However, yet, it only applies to single-phase flow capacity prediction, and its utility diminishes for the highly nonlinear gas-water two-phase flow that occurs during CBM development. The numerical simulation method can handle multiphase fluid flow problems and accurately characterize artificial fractures' parameter characteristics, but it is computationally intensive [30–34]. To achieve high simulation precision, the fractures require grid encryption, which can lead to an extensive mesh network, slowing the calculation speed, especially when dealing with thousands of case studies. Hence, it is of vital importance to develop a dynamic prediction method for gas-water two-phase production in deep CBM reservoirs. Such an approach would not only accurately represent the fracturing network's characteristics in deep CBM reservoirs but also elucidate the seepage flow patterns of gas-water two-phase in these networks. Moreover, it would enable fast and accurate predictions of the production dynamics of the gas-water two-phase.

This study strives to develop a semi-analytical model for predicting the production capacity of deep CBM wells, taking into account the behavior of gas-water two-phase flow. We first construct a physical model for the dynamic analysis of gas-water two-phase production in deep CBM reservoirs, guided by the fundamental characteristics of the fracturing network formed through hydraulic fracturing technology and the gas-water two-phase seepage mechanism within this network. Next, we employ a modified three-linear flow model to represent the fracturing network, wherein complex-induced fractures, coal cleats, and the matrix are approximated as equivalent continuous media. When solving the proposed mathematical model, we explore an efficient method to handle the non-linear seepage flow issue brought about by the two-phase flow of gas and water. We verify the accuracy of our model by contrasting its results with those obtained from commercial numerical simulation software. Furthermore, based on the actual measurement data report of the production wells in the study area, and the semi-analytical solution devised in this study, we analyze the influence of several critical parameters related to fractures and reservoirs on production prediction. There are many factors that affect the productivity of CBM wells, we will continue to study the influence of the sensitivity parameters on rate response in detail in the following study [35–37]. Finally, to demonstrate the practical utility of our proposed method, we conduct production capacity prediction and analysis on a sample well.

2. Methodology

2.1. Physical Model Assumption

In this paper, we adopt a three-linear flow model to reflect the fracturing modifications in deep CBM wells. As depicted in Figure 1, the proposed model entails three distinct regions: the inner zone where fractures exhibit linear flow; the formation fluid's linear flow perpendicular to the fractures; and the outer zone where fluids flow linearly parallel to the fractures [38]. The model presumes that the artificial fracture intersects perpendicularly with the reservoir, intersecting only with the perforation of the horizontal well, while the remaining sections of the horizontal well remain closed. The artificial fracturing is directly linked to the wellbore, and fluids enter the production wellbore solely via

the fracture. Consequently, the fluid of the reservoir continuously flows towards the fracture, replenishing its energy. We also assume that gas and water's two-phase flow takes place in both the fracture network and cleat systems, with the flow behavior adhering to Darcy's law [28,29]. The adsorption of CBM in the coal matrix obeys the Langmuir equation [31], while CBM's diffusion within the coal matrix conforms to Fick's first law, with the pseudo-steady-state diffusion model taken into account [34]. The following simplifying assumptions are adopted for the derivation of the governing equation: (1) The top, bottom, and lateral boundaries of the reservoir are all closed, the distance of external boundary is denoted by y_e ; (2) The fracturing fracture is symmetrical with the wellbore, where the fracture's half-length is denoted by y_F , and the fracture width is w_F ; (3) The permeability of the reservoir is sensitive to stress; (4) The influences of gravity and capillary pressure are not considered.

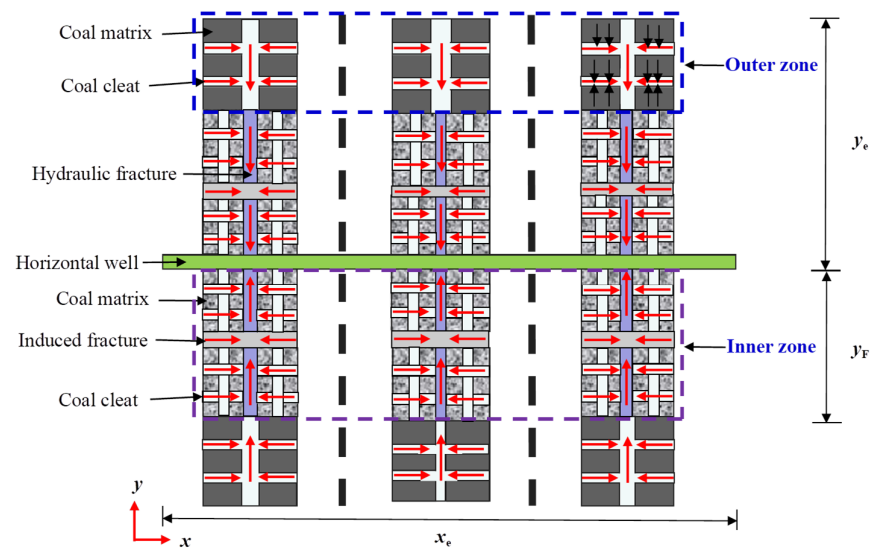


Figure 1. Schematic diagram of fractured horizontal well model in the deep CBM reservoir.

2.2. Mathematical Model

Informed by the presuppositions of the physical model, we devise a mathematical model within this section to elucidate the fluid flow in both the coal reservoir and associated fracture networks. The Langmuir equation is employed to capture the dynamics of CBM adsorption and desorption within the inner and outer zones. To describe CBM diffusion within these regions, we incorporate a pseudo-steady-state diffusion model. Darcy's seepage flow equation provides the framework for portraying the transient flow of gas and water within the cleats and fractures. Following the mechanistic model, mathematical models are correspondingly established for the fluid flow within each of the three distinct flow regions.

2.2.1. Fluid Flow in the Outer Zone

For fluid flow in the outer zone, using pseudo-pressure and pseudo-time, the governing equation for coal gas flow in the cleats is approximately written as:

$$\frac{\partial^2 \psi_{f2}}{\partial x^2} = \frac{1}{0.0864} \left[\frac{\phi_{f2} c_{tf2} \mu}{k_{f2} k_{frg}} \frac{\partial \psi_{f2}}{\partial t} - \frac{\alpha k_m}{k_{f2}} (\psi_m - \psi_{f2}) \right] \quad (1)$$

The flow equation in the coal matrix is written as:

$$-\frac{\alpha k_m}{k_{f2}} (\psi_m - \psi_{f2}) = \frac{\phi_m \mu c_{tmi}}{k_{f2}} \frac{\partial \psi_m}{\partial t} + \frac{2RT}{k_{f2}} \frac{6D\pi^2}{R_m^2} [V_E(\psi_m) - V_m] \quad (2)$$

Coal gas adsorption follows the Langmuir isotherm principle:

$$V_E = \frac{V_L \psi(p)}{\psi_L(p_L) + \psi(p)} \quad (3)$$

Coal gas diffuses in the matrix system obeying Fick's diffusion law. The diffusion equation of shale gas is given by:

$$\frac{\partial V_m}{\partial t} = -3.6D\alpha(V_m - V_E) \quad (4)$$

The initial adsorption amount is:

$$V_m|_{t=0} = V_{Ei}(\psi_i) \quad (5)$$

where, α is the shape factor of the matrix, $1/m^2$; D is the diffusion coefficient, m^2/h ; V_E is the equilibrium adsorption concentration, m^3/m^3 ; V_{Ei} is the equilibrium adsorption concentration at initial condition, m^3/m^3 ; V_L is the Langmuir volume, m^3/m^3 ; p_L is the Langmuir volume, MPa; Ψ_L is the Langmuir pseudo-pressure, MPa/(mPa·s).

To simplify the form of the mathematical model, the dimensionless parameters and definitions are introduced in Table 1.

Table 1. Definition of dimensionless parameters.

Parameters	Symbol	Definition
Dimensionless pseudo pressure of the hydraulic fracture	ψ_{FD}	$\psi_{FD} = \frac{\psi_i - \psi_E}{\psi_i - \psi_w}$
Dimensionless pseudo pressure of the cleat in the outer zone	ψ_{f2D}	$\psi_{f2D} = \frac{\psi_i - \psi_{f2}}{\psi_i - \psi_w}$
Dimensionless pseudo pressure of the cleat in the inner zone	ψ_{f1D}	$\psi_{f1D} = \frac{\psi_i - \psi_{f1}}{\psi_i - \psi_w}$
Dimensionless pseudo pressure of the coal matrix in the outer zone	ψ_{m2D}	$\psi_{m2D} = \frac{\psi_i - \psi_{m2}}{\psi_i - \psi_w}$
Dimensionless pseudo pressure of the coal matrix in the inner zone	ψ_{m1D}	$\psi_{m1D} = \frac{\psi_i - \psi_{m1}}{\psi_i - \psi_w}$
Dimensionless pseudo time	t_{aD}	$t_{aD} = \beta_2 \frac{k_m}{\phi_m \mu_g c_{tm} l_R^2} t_a$
Dimensionless pressure of the hydraulic fracture	p_{FD}	$p_{FD} = \frac{p_i - p_E}{p_i - p_w}$
Dimensionless pressure of the cleat in the outer zone	p_{f2D}	$p_{f2D} = \frac{p_i - p_{f2}}{p_i - p_w}$
Dimensionless pressure of the cleat in the inner zone	p_{f1D}	$p_{f1D} = \frac{p_i - p_{f1}}{p_i - p_w}$
Dimensionless time	t_D	$t_D = \beta_2 \frac{k_m}{\phi_m \mu_g c_{tm} l_R^2} t$
Dimensionless hydraulic fracture conductivity	C_{FD}	$C_{FD} = \frac{k_F \omega_F}{k_m l_R}$
Dimensionless hydraulic fracture pressure transmitting coefficient	η_{FD}	$\eta_{FD} = \frac{k_F}{k_m} \frac{\phi_m c_{tm}}{\phi_E c_{tF}}$
Dimensionless fracture aperture	w_{FD}	$w_{FD} = \frac{\omega_F}{l_R}$
Dimensionless distance in the x direction	x_D	$x_D = \frac{x}{l_R}$
Dimensionless distance in the y direction	y_D	$y_D = \frac{y}{l_R}$
Dimensionless distance in the z direction	z_D	$z_D = \frac{z}{l_R}$
Dimensionless outer boundary in the x direction	x_{eD}	$x_{eD} = \frac{x_e}{l_R}$
Dimensionless outer boundary in the y direction	y_{eD}	$y_{eD} = \frac{y_e}{l_R}$
Dimensionless half-length of the hydraulic fracture	y_{FD}	$y_{FD} = \frac{y_F}{l_R}$
Dimensionless adsorption concentration of the coal matrix	V_{mD}	$V_{mD} = \frac{V_{Ei}(\psi_i) - V_m(\psi)}{V_{Ei}(\psi_i)}$
Dimensionless equilibrium adsorption concentration	V_{ED}	$V_{ED} = \frac{V_{Ei}(\psi_i) - V_E(\psi)}{V_{Ei}(\psi_i)}$
Capacitance coefficient of the coal cleat in the outer zone	ω_2	$\omega_2 = \frac{\phi_{f2} \mu_{g1} c_{tff}}{\sigma}$
Diffusion flow coefficient	λ	$\lambda = \frac{2D\alpha h p_{sc} Tr_w^2 V_{Ei}}{\beta_2 q_{sc} \mu_g l_{sc}}$
Capacitance coefficient of coal cleat in the inner zone	ω_1	$\omega_1 = \frac{\phi_{f1} \mu_{g1} c_{tff}}{\sigma}$
Inter-porosity flow factor of coal matrix system into coal cleat system	λ_{mf}	$\lambda_{mf} = \alpha \frac{k_m}{k_f} l_R^2$

Considering the PVT-dependent properties of the gas phase, the flow equation of the gas phase in the outer zone is treated by pseudo-pressure and pseudo-time. The dimensionless governing equation of the gas phase in the cleat system can be written by:

$$\frac{\partial^2 \psi_{f2D}}{\partial x_D^2} = \frac{1}{\eta_{fD} k_{fD}} \left[\omega_2 \frac{\partial \psi_{f2D}}{\partial t_{aD}} + (1 - \omega_2) \frac{\partial V_{m2D}}{\partial t_{aD}} \right] \quad (6)$$

The pseudo-steady-state diffusion equation of CBM in the outer zone is expressed by:

$$(1 - \omega_2) \frac{\partial V_{m2D}}{\partial t_{aD}} = -\lambda_2 (V_{m2D} - V_{ED}) \quad (7)$$

With the Langmuir isothermal theory, the equation for describing the adsorption of CBM in the outer zone is given below:

$$V_{ED} = \beta \psi_{f2D} \quad (8)$$

The boundary conditions, including the initial, the inner and the external boundaries are given by:

$$\begin{cases} V_{m2D}|_{t_{aD}=0} = 0 \\ \psi_{f2D}(x_D, t_{aD})|_{t_{aD}=0} = 0 \\ \psi_{f2D}(x_D, t_{aD})|_{x_D=1} = \psi_{f1D}(x_D, t_{aD})|_{x_D=1} \\ \frac{\partial \psi_{f2D}(x_D, t_{aD})}{\partial x_D}|_{x_D=x_{eD}} = 0 \end{cases} \quad (9)$$

Because the physical properties of formation water do slightly vary with temperature and pressure, the flow equation of the water phase in the outer zone can be treated by real pressure and time, which is given by:

$$\frac{\partial^2 p_{f2}}{\partial x^2} = \frac{1}{0.0864} \frac{\phi_{f2} c_{ff2} \mu}{k_{f2} k_{frw}} \frac{\partial p_{f2}}{\partial t} \quad (10)$$

Thus, the dimensionless governing equation of the water phase in the cleat system can be written as:

$$\frac{\partial^2 p_{fD}}{\partial x_D^2} = \frac{1}{\eta_{fwD} k_{fwD}} \frac{\partial p_{fD}}{\partial t_D} \quad (11)$$

The boundary conditions are written by:

$$\begin{cases} p_{f2D}(x_D, t_D)|_{t_D=0} = 0 \\ p_{f2D}(x_D, t_D)|_{x_D=1} = p_{f1D}(x_D, t_D)|_{x_D=1} \\ \frac{\partial p_{f2D}(x_D, t_D)}{\partial x_D}|_{x_D=x_{eD}} = 0 \end{cases} \quad (12)$$

where ψ_{f1D} is the dimensionless pseudo-pressure of the cleat system in the inner zone; ψ_{f2D} is the dimensionless pseudo-pressure of the cleat system in the outer zone; p_{f1D} is the pressure of the cleat system in the inner zone; p_{f2D} is the pressure of the cleat system in the outer zone; V_{m2D} is the dimensionless adsorption concentration of the coal matrix in the outer zone; V_{ED} is the dimensionless equilibrium adsorption concentration of the coal matrix in the outer zone; k_{fD} is the relative permeability of the gas phase in the cleat system; k_{frw} is the relative permeability of water phase in the cleat system; x_D is the dimensionless distance in the x direction; x_{eD} is the dimensionless outer boundary distance in the x direction; η_{f2D} is the dimensionless conductivity coefficient of the gas phase in the outer zone cleat system; η_{f2wD} is the dimensionless conductivity coefficient of the water phase in the outer zone cleat system; t_{aD} is the dimensionless pseudo-time; t_D is the dimensionless time; ω_2 is the storage capacity coefficient of the cleat system in the outer zone; λ_2 is the interporosity flow coefficient of the cleat system in the outer zone; β is the adsorption coefficient of CBM.

2.2.2. Fluid Flow in the Inner Zone

The complex fracture network in the inner zone is composed of micro-fractures, secondary fractures and hydraulic fractures. In this section, a dual-porosity model is modified to capture the transient flow of the micro-fractures and secondary fractures. Using pseudo-pressure and pseudo-time, the dimensionless governing equation of the gas phase in the fracture systems of the inner zone is given by:

$$\frac{\partial}{\partial y} \left(\frac{p_{f1}}{Z} \cdot \frac{k_{f1} k_{frg}}{\mu} \frac{\partial p_{f1}}{\partial y} \right) = \frac{1}{0.0864} \left[\frac{\partial \left(\frac{p_f}{Z} S_{f1g} \phi_{f1} \right)}{\partial t} - \frac{\alpha k_m}{k_{f1}} (\psi_m - \psi_{f1}) \right] \quad (13)$$

The dimensionless governing equation of the gas phase in the inner zone is written as:

$$\frac{\partial^2 \psi_{f1D}}{\partial y_D^2} + \frac{1}{k_{frg}} \frac{\partial \psi_{f2D}}{\partial x_D} \Big|_{x_D=1} = \frac{1}{\eta_{f1D} k_{frg}} \left[\omega_1 \frac{\partial \psi_{f1D}}{\partial t_{aD}} + (1 - \omega_1) \frac{\partial V_{m1D}}{\partial t_{aD}} \right] \quad (14)$$

The pseudo-steady-state diffusion equation of CBM in the inner zone is given by:

$$(1 - \omega_1) \frac{\partial V_{m1D}}{\partial t_{aD}} = -\lambda_1 (V_{m1D} - V_{eD}) \quad (15)$$

According to the Langmuir isothermal adsorption law, the equation for describing the adsorption of CBM in the inner zone is:

$$V_{eD} = \beta \psi_{f1D} \quad (16)$$

The boundary conditions of the inner zone are given by:

$$\begin{cases} V_{m1D} \Big|_{t_{aD}=0} = 0 \\ \psi_{f1D}(y_D, t_{aD}) \Big|_{t_{aD}=0} = 0 \\ \psi_{f1D}(y_D, t_{aD}) \Big|_{y_D=w_{FD}/2} = \psi_{FD} \\ \frac{\partial \psi_{f1D}(y_D, t_{aD})}{\partial y_D} \Big|_{y_D=y_{eD}} = 0 \end{cases} \quad (17)$$

The flow equation of the water phase in the inner zone is treated with real pressure and real-time, and the dimensionless governing equation is:

$$\frac{\partial^2 p_{f1D}}{\partial y_D^2} + \frac{1}{k_{frw}} \frac{\partial p_{f2D}}{\partial x_D} \Big|_{x_D=1} = \frac{1}{\eta_{f1D} k_{frw}} \frac{\partial p_{f1D}}{\partial t_D} \quad (18)$$

The boundary conditions are given by:

$$\begin{cases} p_{f1D}(y_D, t_D) \Big|_{t_D=0} = 0 \\ p_{f1D}(y_D, t_D) \Big|_{y_D=w_{FD}/2} = p_{FD} \\ \frac{\partial p_{f1D}(y_D, t_D)}{\partial y_D} \Big|_{y_D=y_{eD}} = 0 \end{cases} \quad (19)$$

2.2.3. Fluid Flow in the Hydraulic Fractures

In this paper, a two-phase flow of gas and water is considered in hydraulic fractures. Using the pseudo-pressure and pseudo-time, the gas flow equation in the hydraulic fracture is written by:

$$\frac{\partial^2 \psi_F}{\partial x^2} = \frac{1}{0.0864} \frac{\phi_F c_{tF} \mu}{k_F k_{Frg}} \frac{\partial \psi_F}{\partial t} - \frac{2k_{f1} k_{frg}}{w_F k_F k_{Frg}} \frac{\partial \psi_{f1}}{\partial y} \Big|_{y_D=w_F/2} \quad (20)$$

The dimensionless governing equation is written as:

$$\frac{\partial^2 \psi_{FD}}{\partial x_D^2} + \frac{2k_{frg}}{C_{FD}k_{FrG}} \frac{\partial \psi_{f1D}}{\partial y_D} \Big|_{y_D=w_{FD}/2} = \frac{1}{\eta_{FD}k_{FrG}} \frac{\partial \psi_{FD}}{\partial t_{aD}} \quad (21)$$

The boundary conditions are expressed as:

$$\begin{cases} \psi_{FD}(x_D, t_{aD}) \Big|_{t_{aD}=0} = 0 \\ \psi_{FD}(x_D, t_{aD}) \Big|_{x_D=0} = 1 \\ \frac{\partial \psi_{FD}}{\partial x_D} \Big|_{x_D=1} = 0 \end{cases} \quad (22)$$

The water phase flow equation is given by:

$$\frac{\partial^2 p_F}{\partial x^2} = \frac{1}{0.0864} \frac{\phi_{FCtF}\mu}{k_F k_{FrW}} \frac{\partial p_F}{\partial t} - \frac{2k_{f1}k_{frw}}{w_F k_F k_{FrW}} \frac{\partial p_{f1}}{\partial y} \Big|_{y_D=w_F/2} \quad (23)$$

The dimensionless governing equation can be written by:

$$\frac{\partial^2 p_{FD}}{\partial x_D^2} + \frac{2k_{frw}}{C_{FD}k_{FrW}} \frac{\partial p_{f1D}}{\partial y_D} \Big|_{y_D=w_{FD}/2} = \frac{1}{\eta_{FD}k_{FrW}} \frac{\partial p_{FD}}{\partial t_D} \quad (24)$$

The boundary conditions are:

$$\begin{cases} p_{FD}(x_D, t_D) \Big|_{t_D=0} = 0 \\ p_{FD}(x_D, t_D) \Big|_{x_D=0} = 1 \\ \frac{\partial p_{FD}}{\partial x_D} \Big|_{x_D=1} = 0 \end{cases} \quad (25)$$

where C_{FD} is the dimensionless conductivity of the hydraulic fracture; η_{FD} is the dimensionless conductivity coefficient of the gas phase in the hydraulic fracture system; η_{FDW} is the dimensionless conductivity coefficient of the water phase in the hydraulic fracture system; w_{FD} is the dimensionless width of the hydraulic fracture; k_{FrG} is the relative permeability of the gas phase in the hydraulic fracture system; k_{FrW} is the relative permeability of the water phase in the hydraulic fracture system.

2.3. Solution to Mathematical Model

Because the parameters including μ_g , B_g , k_{FrG} , k_{frg} , k_{mrg} , k_{FrW} , k_{frw} and k_{mrw} are functions of the pressure and saturation, it is difficult to derive the analytical solution of the proposed mathematical model directly. In this paper, an effective and accurate semi-analytical method is presented to solve the problem. In our approach, the production time is discretized into several time steps, and at each time step, the pressure-dependent parameters (μ_g , B_g) and the saturation-dependent parameters (k_{mrg} , k_{mrw} , k_{frg} , k_{frw} , k_{FrG} , k_{FrW}) are updated by the average pressure and average saturation, respectively. The average pressure and saturation are calculated by using the material balance method. Therefore, the nonlinear parameters can be regarded as fixed approximations at each time step, and the nonlinear problems can be converted to linear problems through this method. Thus, the solution of the proposed model can be obtained with the Laplace transformation method directly. In the following sections, the analytical solutions for gas and water production are presented, respectively.

2.3.1. Solution for Gas and Water Flow in the Outer Zone

Using the Laplace transformation, the solution of the outer zone flow model can be obtained and the general solution for Equation (6) is given by:

$$\bar{\psi}_{i2D} = A \sinh \left(\sqrt{\frac{f_2(u)}{\eta_{FD}k_{frg}}} \cdot x_D \right) + B \cosh \left(\sqrt{\frac{f_2(u)}{\eta_{FD}k_{frg}}} \cdot x_D \right) \quad (26)$$

$$f_2(u) = u\omega_2 + u(1 - \omega_2) \frac{\lambda_2\beta}{u(1 - \omega_2) + \lambda_2} \quad (27)$$

Substituting Equation (9) into Equation (26), one can obtain

$$A = \frac{\sinh\left(\sqrt{\frac{f_2(u)}{\eta_{fD}k_{frg}}} \cdot x_{eD}\right) \cdot \bar{\psi}_{f1D}}{\sinh\left(\sqrt{\frac{f_2(u)}{\eta_{fD}k_{frg}}}\right) \sinh\left(\sqrt{\frac{f_2(u)}{\eta_{fD}k_{frg}}} \cdot x_{eD}\right) - \cosh\left(\sqrt{\frac{f_2(u)}{\eta_{fD}k_{frg}}}\right) \cosh\left(\sqrt{\frac{f_2(u)}{\eta_{fD}k_{frg}}} \cdot x_{eD}\right)} \quad (28)$$

$$B = \frac{-\cosh\left(\sqrt{\frac{f_2(u)}{\eta_{fD}k_{frg}}} \cdot x_{eD}\right) \cdot \bar{\psi}_{f1D}}{\sinh\left(\sqrt{\frac{f_2(u)}{\eta_{fD}k_{frg}}}\right) \sinh\left(\sqrt{\frac{f_2(u)}{\eta_{fD}k_{frg}}} \cdot x_{eD}\right) - \cosh\left(\sqrt{\frac{f_2(u)}{\eta_{fD}k_{frg}}}\right) \cosh\left(\sqrt{\frac{f_2(u)}{\eta_{fD}k_{frg}}} \cdot x_{eD}\right)} \quad (29)$$

The general solution for Equation (11) in the Laplace domain is given as:

$$\bar{p}_{f2D} = A_1 \sinh\left(\sqrt{\frac{u}{\eta_{fwD}k_{frw}}} \cdot x_D\right) + B_1 \cosh\left(\sqrt{\frac{u}{\eta_{fwD}k_{frw}}} \cdot x_D\right) \quad (30)$$

Substituting Equation (12) into Equation (30), one can obtain

$$A_1 = \frac{\sinh\left(\sqrt{\frac{u}{\eta_{fwD}k_{frw}}} \cdot x_{eD}\right) \cdot \bar{p}_{f1D}}{\sinh\left(\sqrt{\frac{u}{\eta_{fwD}k_{frw}}}\right) \sinh\left(\sqrt{\frac{u}{\eta_{fwD}k_{frw}}} \cdot x_{eD}\right) - \cosh\left(\sqrt{\frac{u}{\eta_{fwD}k_{frw}}}\right) \cosh\left(\sqrt{\frac{u}{\eta_{fwD}k_{frw}}} \cdot x_{eD}\right)} \quad (31)$$

$$B_1 = \frac{-\cosh\left(\sqrt{\frac{u}{\eta_{fwD}k_{frw}}} \cdot x_{eD}\right) \cdot \bar{p}_{f1D}}{\sinh\left(\sqrt{\frac{u}{\eta_{fwD}k_{frw}}}\right) \sinh\left(\sqrt{\frac{u}{\eta_{fwD}k_{frw}}} \cdot x_{eD}\right) - \cosh\left(\sqrt{\frac{u}{\eta_{fwD}k_{frw}}}\right) \cosh\left(\sqrt{\frac{u}{\eta_{fwD}k_{frw}}} \cdot x_{eD}\right)} \quad (32)$$

where, $\bar{\psi}_{f1D}$ is the dimensionless pseudo-pressure of the inner zone cleat system in the Laplace domain; $\bar{\psi}_{f2D}$ is the dimensionless pseudo-pressure of the outer zone cleat system in the Laplace domain; \bar{p}_{f1D} is the dimensionless pressure of the inner zone cleat system in the Laplace domain; \bar{p}_{f2D} is the dimensionless pressure of the outer zone cleat system in the Laplace domain; u is the Laplace constant.

2.3.2. Solution for Gas and Water Flow in the Inner Zone

The solving method for gas and water flow in the inner zone is similar to that of the outer zone flow model. We perform the Laplace transformation on the equation of gas and water phase in the inner zone. Combined with Equation (26), the solution of the inner zone flow model can be obtained and the general solution for Equation (14) is expressed by:

$$\bar{\psi}_{f1D} = C \sinh(\sqrt{\sigma} \cdot y_D) + D \cosh(\sqrt{\sigma} \cdot y_D) \quad (33)$$

$$\sigma = \left[\sqrt{\frac{f_1(u)}{\eta_{fD}k_{frg}}} + \frac{1}{k_{frg}} \sqrt{\frac{f_2(u)}{\eta_{fD}k_{frg}}} \tanh \sqrt{\frac{f_2(u)}{\eta_{fD}k_{frg}}} (x_{eD} - 1) \right] \quad (34)$$

Substituting the boundary conditions Equation (17) into Equation (33), one can obtain

$$C = \frac{\sinh(\sqrt{\sigma} \cdot y_{eD}) \cdot \bar{\psi}_{FD}}{\sinh(\sqrt{\sigma}) \sinh(\sqrt{\sigma} \cdot y_{eD}) - \cosh(\sqrt{\sigma}) \cosh(\sqrt{\sigma} \cdot y_{eD})} \quad (35)$$

$$D = \frac{-\cosh(\sqrt{\sigma} \cdot y_{eD}) \cdot \bar{\psi}_{FD}}{\sinh(\sqrt{\sigma}) \sinh(\sqrt{\sigma} \cdot y_{eD}) - \cosh(\sqrt{\sigma}) \cosh(\sqrt{\sigma} \cdot y_{eD})} \quad (36)$$

Combined with the solution for water flow in the outer zone, the general solution for Equation (18) in the Laplace domain is given by:

$$\bar{p}_{f1D} = C_1 \sinh(\sqrt{\delta} \cdot y_D) + D_1 \cosh(\sqrt{\delta} \cdot y_D) \quad (37)$$

$$\delta = \left[\sqrt{\frac{u}{\eta_{fwD} k_{frw}}} + \frac{1}{k_{frw}} \sqrt{\frac{u}{\eta_{fwD} k_{frw}}} \tanh \sqrt{\frac{u}{\eta_{fwD} k_{frw}}} (x_{eD} - 1) \right] \quad (38)$$

Substituting Equation (30) and the boundary conditions Equation (19) into Equation (37), one can obtain

$$C_1 = \frac{\sinh(\sqrt{\delta} \cdot y_{eD}) \cdot \bar{p}_{FD}}{\sinh(\sqrt{\delta}) \sinh(\sqrt{\delta} \cdot y_{eD}) - \cosh(\sqrt{\delta}) \cosh(\sqrt{\delta} \cdot y_{eD})} \quad (39)$$

$$D_1 = \frac{-\cosh(\sqrt{\delta} \cdot y_{eD}) \cdot \bar{p}_{FD}}{\sinh(\sqrt{\delta}) \sinh(\sqrt{\delta} \cdot y_{eD}) - \cosh(\sqrt{\delta}) \cosh(\sqrt{\delta} \cdot y_{eD})} \quad (40)$$

where, $\bar{\psi}_{FD}$ is the dimensionless pseudo-pressure of the hydraulic fracture in the Laplace domain; \bar{p}_{FD} is the dimensionless pressure of the hydraulic fracture in the Laplace domain.

2.3.3. Solution for Gas and Water Flow in the Hydraulic Fracture

With Laplace transformation, the solution of the hydraulic fracture flow model can be obtained and the general solution for Equation (21) is expressed as:

$$\bar{\psi}_{FD} = -\frac{1}{u} (\tanh \sqrt{\alpha} \sinh \sqrt{\alpha} x_D - \cosh \sqrt{\alpha} x_D) \quad (41)$$

$$\alpha = \frac{u}{\eta_{FD} k_{FrG}} + \frac{2k_{frg}}{C_{FD} k_{FrG}} \sqrt{\sigma} \tanh \sqrt{\sigma} \left(y_{eD} - \frac{w_{FD}}{2} \right) \quad (42)$$

Combined with the solution for water flow in the inner zone, the general solution for Equation (24) in the Laplace domain is given by:

$$\bar{p}_{FD} = -\frac{1}{u} (\tanh \sqrt{\zeta} \sinh \sqrt{\zeta} x_D - \cosh \sqrt{\zeta} x_D) \quad (43)$$

$$\zeta = \frac{u}{\eta_{FwD} k_{Frw}} + \frac{2k_{frw}}{C_{FD} k_{Frw}} \sqrt{\delta} \tanh \sqrt{\delta} \left(y_{eD} - \frac{w_{FD}}{2} \right) \quad (44)$$

The gas production rate is:

$$\bar{q}_{gD} = -\frac{k_{FD} k_{FrG} w_{FD}}{\pi} \frac{\partial \bar{\psi}_{FD}}{\partial x_D} \Big|_{x_D=0} \quad (45)$$

According to Equation (45), the solution of the gas production rate becomes:

$$\bar{q}_{gD} = -\frac{k_{FD} k_{FrG} w_{FD}}{\pi} \frac{1}{u} \sqrt{\alpha} \tanh \sqrt{\alpha} \quad (46)$$

The water production rate is:

$$\bar{q}_{wD} = -\frac{k_{FD} k_{Frw} w_{FD}}{\pi} \frac{\partial \bar{p}_{FD}}{\partial x_D} \Big|_{x_D=0} \quad (47)$$

According to Equation (47), the solution of the water production rate becomes:

$$\bar{q}_{wD} = -\frac{k_{FD}k_{Frw}w_{FD}}{\pi} \frac{1}{u} \sqrt{\xi} \tanh \sqrt{\xi} \quad (48)$$

In this paper, the stress-sensitive terms are all integrated into the conductivity, and as a function of the average formation pressure. The theoretical formula for describing the effect of the stress-sensitive is defined as [38]:

$$k_f = k_{fi} e^{-\gamma(p_i - \hat{p})} \quad (49)$$

where, k_f is the permeability of the cleat system, mD; k_{fi} is the initial permeability of the cleat system, mD; γ is the permeability modulus, MPa^{-1} ; p_i is the original formation pressure, MPa; \hat{p} is the average formation pressure, MPa.

2.3.4. Flowing Material Balance Method

As mentioned in Section 2.3 of this paper, at each time step, the pressure-related parameters (μ_g, B_g) and saturation-related parameters ($k_{mrg}, k_{mrw}, k_{frg}, k_{frw}, k_{FRg}, k_{FRw}$) in the gas-water two-phase production solution and the stress-sensitive terms are updated by the average pressure and average saturation within the investigated range, while the average formation pressure and average saturation are calculated using the flowing material balance method. In this section, the process of establishing the flowing material balance equations of gas-water two-phase is presented.

For a single fracture stage, the mass equilibrium equation for the gas phase can be written as:

$$x_{inv} H y_{inv} \phi_m \left(\frac{S_{gi}}{B_{gi}} \right) - x_{inv} H y_{inv} \phi_m \left(\frac{\hat{S}_g}{\hat{B}_g} \right) = \int_0^t q_g dt \quad (50)$$

The mass equilibrium equation for the water phase can be expressed as:

$$x_{inv} H y_{inv} \phi_m \left(\frac{S_{wi}}{B_{wi}} \right) - x_{inv} H y_{inv} \phi_m \left(\frac{\hat{S}_w}{\hat{B}_w} \right) = \int_0^t q_w dt \quad (51)$$

The investigated range for the transient flow in the inner zone is given by [38]:

$$x_{inv} = 0.5836 \sqrt{\frac{k_f t}{\phi_f \mu_g c_t}} + y_F \quad (52)$$

$$y_{inv} = 0.5836 \sqrt{\frac{k_f t}{\phi_f \mu_g c_t}} \quad (53)$$

The saturation relationship between the gas and water phase is:

$$\hat{S}_g + \hat{S}_w = 1 \quad (54)$$

Combining Equations (50)–(54), the average pressure function can be derived as:

$$f(\hat{p}) = \frac{1}{\hat{B}_g} + \left(-\frac{\hat{B}_w}{\hat{B}_g} \right) A_3 - B_3 \quad (55)$$

$$A_3 = \frac{S_{wi}}{B_{wi}} - \frac{\int_0^t q_w dt}{x_{inv} H y_{inv} \phi_m} \quad (56)$$

$$B_3 = \frac{S_{gi}}{B_{gi}} - \frac{\int_0^t q_g dt}{x_{inv} H y_{inv} \phi_m} \quad (57)$$

The Newton iteration is used to update the dynamic parameters by coupling the flowing material balance equations, which is given by:

$$\hat{p}_{k+1} = \hat{p}_k - \chi \frac{f(\hat{p}_k)}{f'(\hat{p}_k)} \quad (58)$$

where S_{gi} is the initial gas saturation; \hat{S}_g is the average gas saturation; S_{wi} is the initial water saturation; \hat{S}_w is the average water saturation; B_{gi} is the initial gas volume factor; \hat{B}_g is the average gas volume factor; B_{wi} is the initial formation water volume factor; \hat{B}_w is the average formation water volume factor; x_{inv} is the investigated range along the fracture direction in the inner zone; y_{inv} is the investigated range perpendicular to the fracture direction in the inner zone; ϕ_m is the matrix porosity; H is the formation thickness; y_F is the fracture half-length; t is the production time; q_g is the gas production rate; q_w is the water production rate; c_t is the total formation compressibility factor.

3. Results and Discussion

3.1. Model Validation

To verify the accuracy of the proposed semi-analytical model, a numerical model was established using the commercial simulation software Eclipse (2019), as shown in Figure 2. Table 2 presents the reservoir and fracture parameters used in both methods, and Figure 3 shows the relative permeability curves of the gas-water two-phase flow in the CBM reservoir and the hydraulic fractures. The selection of parameters in Table 2 is obtained through the actual measurement data report of the production well in the study area. Parameters such as Langmuir volume, Langmuir pressure, and coal gas content, etc. can be obtained through gas content reports; parameters such as reservoir original pressure, pressure gradient, temperature, permeability, etc. can be obtained from injection/fall-off well testing report; parameters such as fracture length and fracture direction can be obtained from micro-fracture monitoring report. In this case study, both the coal cleats and the artificial fractures are considered to have gas-water two-phase flow from the early production stage.

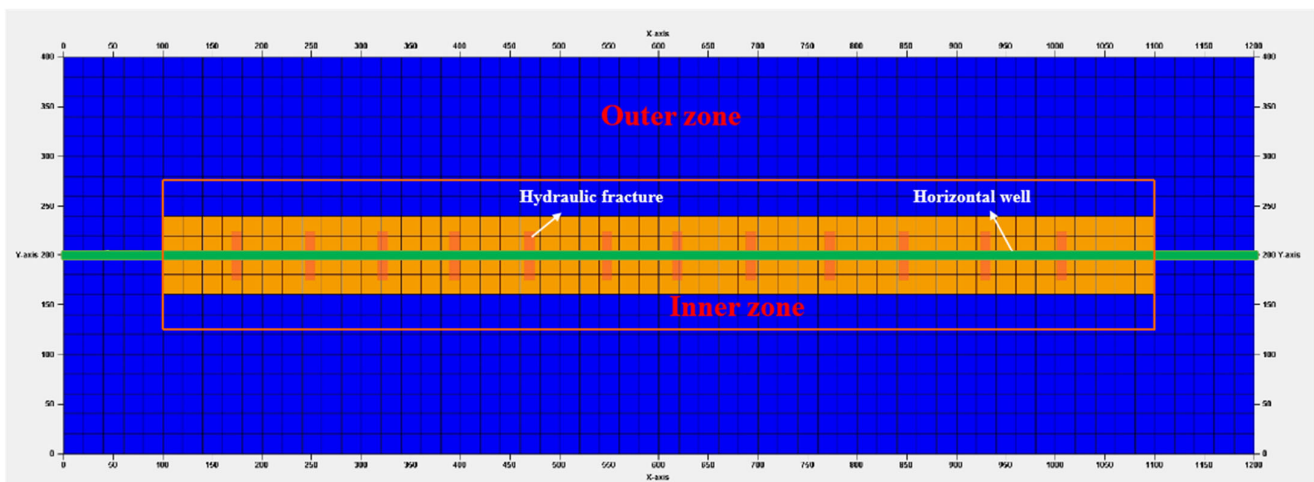
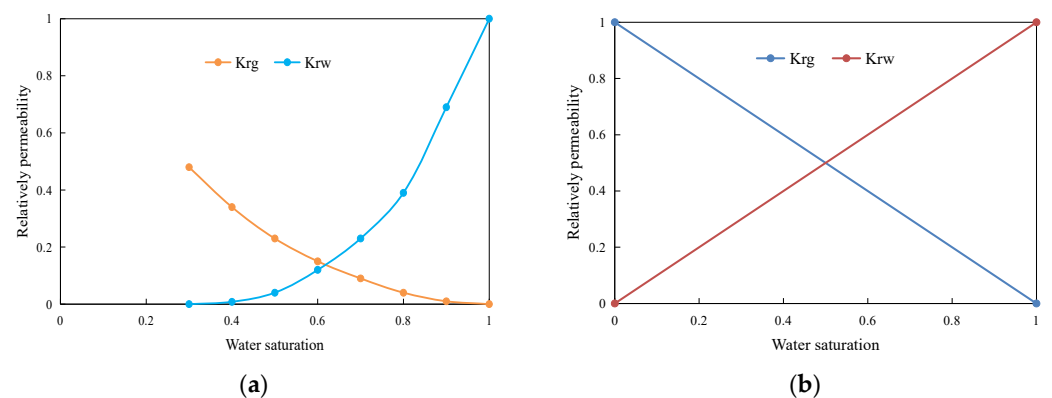


Figure 2. Schematic of the numerical model for a hydraulically fractured horizontal well in the deep CBM reservoir.

Table 2. Input parameters for model validation.

Parameters	Symbol	Units	Value
Initial formation pressure	p_i	MPa	20
Initial formation temperature	T_i	K	323
Bottom-hole pressure	p_{wf}	MPa	4
Formation thickness	h	m	9.1
Permeability of hydraulic fractures	k_F	mD	500
Number of hydraulic fractures	N_F	Dimensionless	12
Half length of hydraulic fractures	y_F	m	100
Width of hydraulic fractures	w_F	m	0.001
Porosity of hydraulic fractures	Φ_F	Fraction	0.4
Length of the horizontal well	L	m	1000
Half-width of the reservoir	y_e	m	200
Porosity of the coal cleat	Φ_f	Fraction	0.05
Permeability of the coal cleat in the inner reservoir	k_f	mD	0.22
Permeability of the outer reservoir	k_o	mD	0.12
Permeability modulus of the coal cleat	γ_f	MPa ⁻¹	0.02
Langmuir pressure	p_L	MPa	3.1
Langmuir volume	V_L	m ³ /t	12.9
Gas content in coal seams	V	m ³ /t	14.8

**Figure 3.** Gas-water relative permeability curves used for model validation. (a) Relative permeability curve in the reservoir. (b) Relative permeability curve in the hydraulic fracture.

The comparison results between the semi-analytical model proposed in this paper and Eclipse are shown in Figure 4. It can be seen that there are some differences in the production curves obtained by the two methods in the early production stage, but the results are basically consistent in the later stage. This is mainly because, in the early production stage, the pressure and saturation in the near wellbore zone change greatly, and production is very sensitive to parameters related to pressure and saturation. In the semi-analytical model, some parameters related to pressure are implicitly handled using a pseudo-pressure approach, but parameters related to saturation are explicitly handled. Therefore, the early errors in the single-phase flow model are not obvious, while the errors in the two-phase flow model are more significant. However, the calculated average relative error is less than 10%, which is within the allowable engineering error range, indicating that the semi-analytical model proposed in this paper can be used for production data analysis and prediction. We should admit that numerical simulation is a powerful tool for evaluating the performance of CBM Wells. However, the process of establishing such fracture networks using commercial numerical simulation software is relatively complex. In addition, the use of localized refinement or non-uniform grids can lead to an increase in the number of grids and significant differences in size between grids, thereby substantially reducing calculation efficiency. Conventional analytical models are often used to model the flow behavior of fractured wells. However, the traditional analytical models are limited

to single-phase flow problems, and seldom consider the combined effect of hydraulic fractures, induced fractures, coal cleats, and the matrix, leading to considerable errors in productivity prediction. The proposed semi-analytical method in this paper is based on the linear flow assumption, effective in depicting the fracturing mesh modification body and expedient for calculations. In addition, when solving the proposed mathematical model, we explore an efficient method to handle the non-linear seepage flow issue brought about by the two-phase flow of gas and water. Employing the flowing material balance method for computing the average pressure and average saturation of the reservoir, and iteratively updating the non-linear parameters in the seepage model, facilitates the accurate handling of the non-linear seepage problem associated with gas-water dual-phase flow. The proposed semi-analytical model captures the flow behavior in the hydraulic fracture network and coal reservoir, and has much higher computational efficiency than numerical simulation methods. This is because the fracture and matrix systems do not need to be divided into meshes. In addition, the solution is not limited by the time step, so the early simulation accuracy is better and the computational efficiency is higher. To obtain the calculation results shown in Figure 4, the proposed semi-analytical method developed in this study was used to calculate on the same platform, and the time was less than 5 s, while Eclipse's calculation time was more than 200 s. Compared with numerical simulation methods, the semi-analytical method proposed in this paper has a faster calculation speed and is more suitable for large-scale case analysis and application in mining fields.

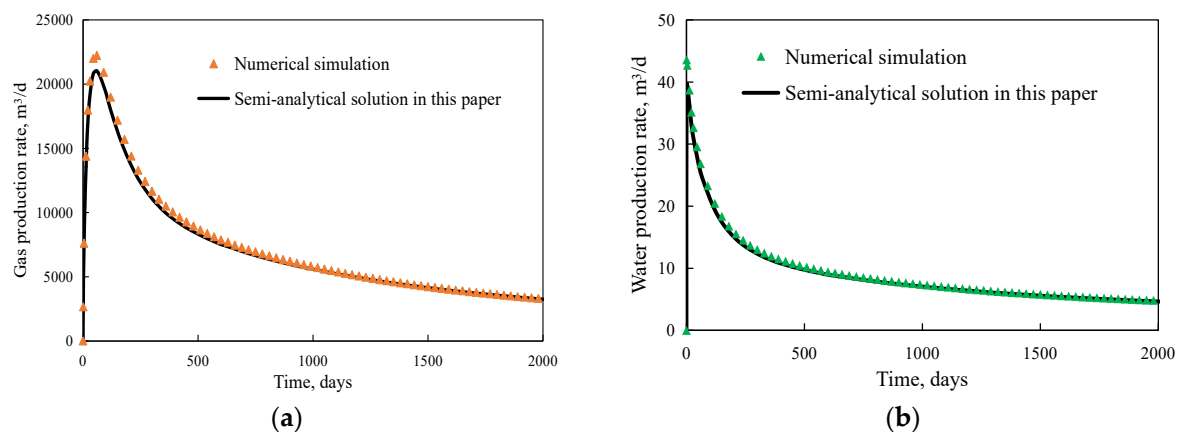


Figure 4. Comparison of gas and water rate between the semi-analytical model in this paper and the Eclipse. (a) Gas rate validation with the numerical solution. (b) Water rate validation with the numerical solution.

The main difference between the proposed model and the traditional analytical models is that the two-phase flow behaviour is incorporated in the proposed model. In this section, we simultaneously simulated the rate transients of both the proposed and conventional analytical models using the same group of formation and well parameters in Table 2. The initial water saturation in the cleats and the hydraulic fractures are given 1 and 0 in the proposed and conventional models, respectively. The modelling results are shown in Figure 5. It is shown that two-phase flow in the cleat and hydraulic fracture systems significantly influences the gas production rate during the whole production period. In addition, the gas production rate is smaller if the water-phase flow is considered in the two systems. This is possible because the gas production from the coal matrix acts as a displacement effect for the limited water in the cleat and hydraulic fracture systems, so the two-phase flow in the cleat and hydraulic fracture systems affects the gas production during the whole period. Besides, the gas production rate will be overestimated without considering the two-phase flow in the cleats and hydraulic fractures.

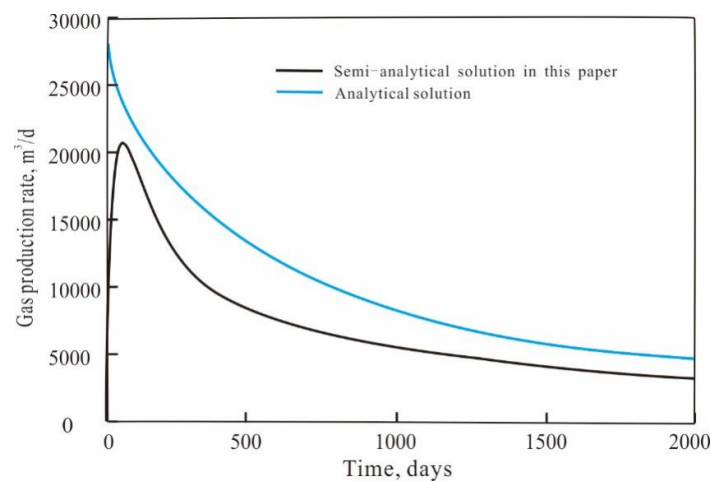


Figure 5. Comparison of gas production rate between the proposed semi-analytical model and the analytical model.

3.2. Sensitivity Analysis

Given the inherently low natural productivity of deep coal reservoirs, hydraulic fracturing has emerged as a pivotal strategy to augment production. Drawing from the investigation into the semi-analytical model, this paper scrutinizes the influence of both the artificial fracturing capacity and the fracture half-length on the production capacity of deep CBM wells. Moreover, grounded in the empirical research findings of the reservoir seepage mechanism, we assess the impact of reservoir properties and stress sensitivity on the production capacity of both gas and water phases. The basic input parameters integral to the model are delineated in Table 2, while Table 3 illustrates the range of sensitivity parameters. The selection of parameters in Table 3 is obtained through the actual measurement data report of the production wells in the study area. According to previous fracturing reports and actual well production performance, the number of hydraulic fractures generally ranges from 8 to 16, and the half-length of hydraulic fractures is generally between 50 to 120 m. In addition, due to the strong heterogeneity of coal reservoirs, it was found through well testing on multiple wells within the same block that the range of permeability of the coal cleat in the inner reservoir is from 0.1 mD to 0.5 mD, and the range of permeability of the outer reservoir is between 0.1 mD and 0.5 mD, and the range of permeability modulus of the coal cleat is from 0.01 MPa⁻¹ to 0.04 MPa⁻¹. Therefore, parameters of conductivity of hydraulic fractures, half length of hydraulic fractures, number of hydraulic fractures, permeability of the coal cleat in the inner reservoir, permeability of the outer reservoir, and permeability modulus of the coal cleat used for sensitivity analysis are shown in Table 3.

Table 3. Parameters used for sensitivity analysis.

Parameters	Symbol	Units	Value
Conductivity of hydraulic fractures	η_F	mD·m	0.3, 0.5, 1
Half length of hydraulic fractures	y_F	m	50, 80, 100
Number of hydraulic fractures	N_F	Dimensionless	9, 12, 15
Permeability of the coal cleat in the inner reservoir	k_f	mD	0.2, 0.3, 0.4
Permeability of the outer reservoir	k_o	mD	0.1, 0.2, 0.3
Permeability modulus of the coal cleat	γ_f	MPa ⁻¹	0.01, 0.02, 0.03

Figure 6 shows the influence of fracture conductivity on the gas productivity of deep CBM wells. It becomes apparent that an increased fracture diversion capacity results in both a higher initial production rate and a more gradual production decline. The primary cause of this is that greater fracture diversion capacity yields elevated production rates.

Under conditions of constant bottom-hole flowing pressure production, a more moderate production decline is adequate to sustain production.

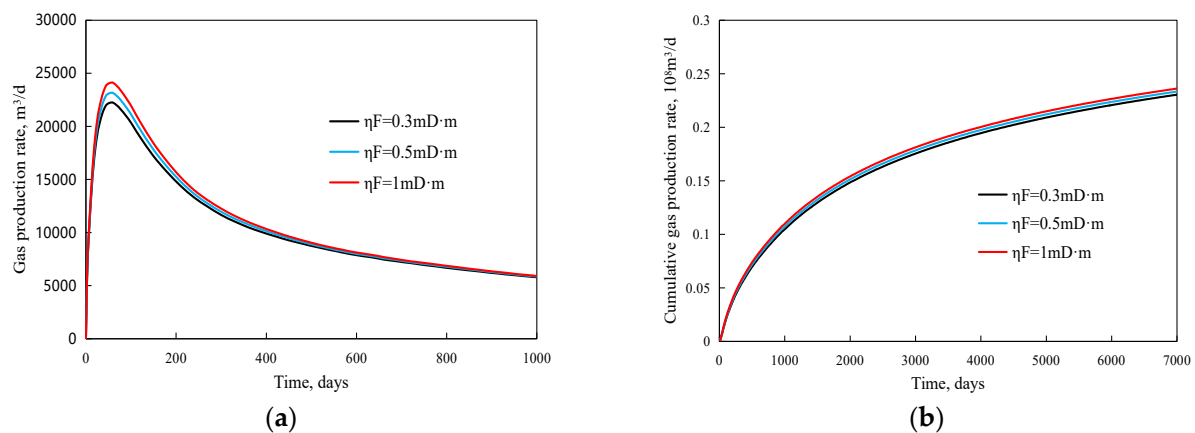


Figure 6. Effect of fracture conductivity on gas production rate. (a) Influence of ηF on gas production rate. (b) Influence of ηF on cumulative gas production rate.

Figure 7 illustrates the impact of fracture half-length on the gas productivity of deep CBM wells. It conveys that alterations in fracture half-length influence the entire development stage, particularly during the initial and intermediate production phases. Moreover, gas production increases with the expansion of the fracture half-length, albeit at a progressively diminishing rate. This is chiefly attributed to the fact that fracture half-length not only signifies the extent of reservoir stimulation volume but also mirrors the well-regulated reserves and drainage area. A more substantial fracture half-length equates to a larger linear flow area of the fracture and an increased drainage area, which in turn leads to higher production rates and a more gradual production decline.

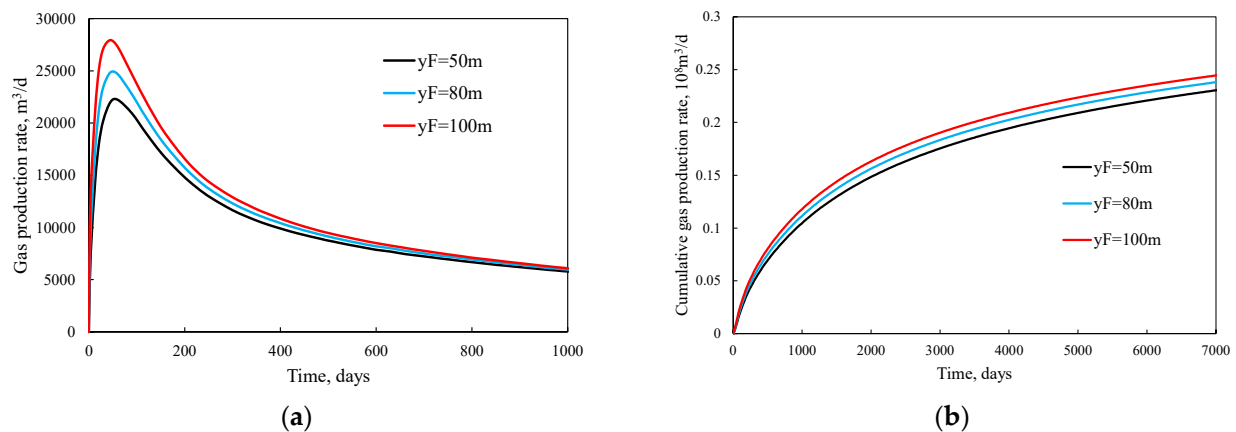


Figure 7. Effect of fracture half-length on gas production rate. (a) Influence of yF on gas production rate. (b) Influence of yF on cumulative gas production rate.

Figure 8 demonstrates the influence of the number of hydraulic fracturing stages on the gas production capacity of deep CBM wells. The diagram clearly indicates that the quantity of hydraulic fracturing stages substantially impacts production. An increase in the number of hydraulic fracturing stages results in a greater initial production capacity and cumulative production. This phenomenon is primarily due to the fact that an increased number of fracturing stages, accompanied by reduced intervals between them, amplifies the pressure drop in the inner zone, stimulating the desorption of adsorbed gas. Moreover, an increased number of fracturing stages also enhances the contact area between artificial fractures and reservoirs, resulting in an increase in production. However, it is worth noting

that the augmentation in production capacity progressively diminishes as the number of fracturing stages increases.

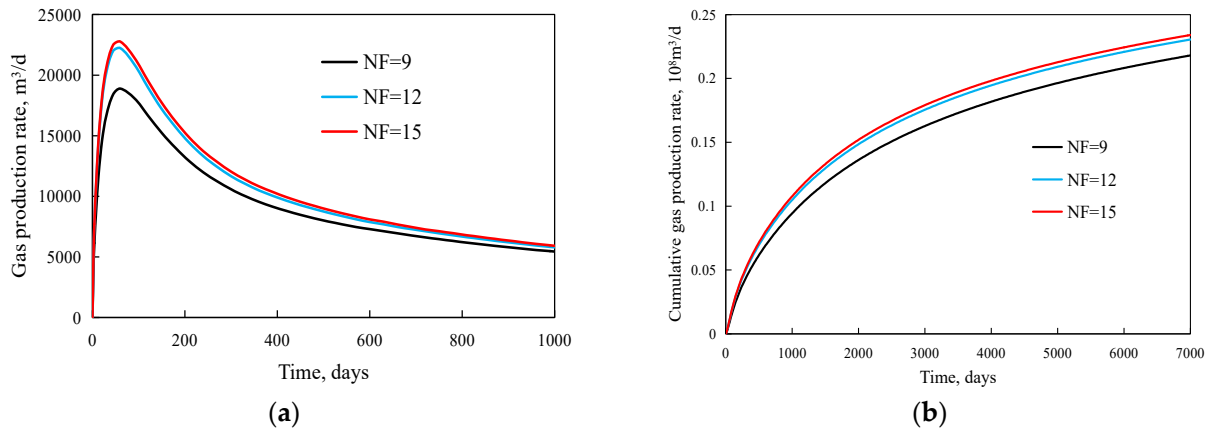


Figure 8. Effect of number of hydraulic fracturing stages on gas production rate. (a) Influence of NF on gas production rate. (b) Influence of NF on cumulative gas production rate.

Figure 9 illustrates the impact of the permeability of the coal cleat in the inner reservoir on the gas production capacity of deep CBM wells. The figure clearly demonstrates that higher coal cleat permeability in the inner reservoir results in greater initial production capacity and cumulative production. The primary reason for this is that an increase in the permeability of the coal cleat in the inner reservoir simultaneously enhances the flow capacity of free gas and desorption. As a result, the ease with which a pressure drop influences the interior of the inner zone matrix is increased, stimulating the desorption of adsorbed gas in the inner zone. Moreover, as the permeability of the coal cleat in the inner reservoir increases, the gas in the inner zone finds it increasingly conducive to flow towards secondary and artificial fractures.

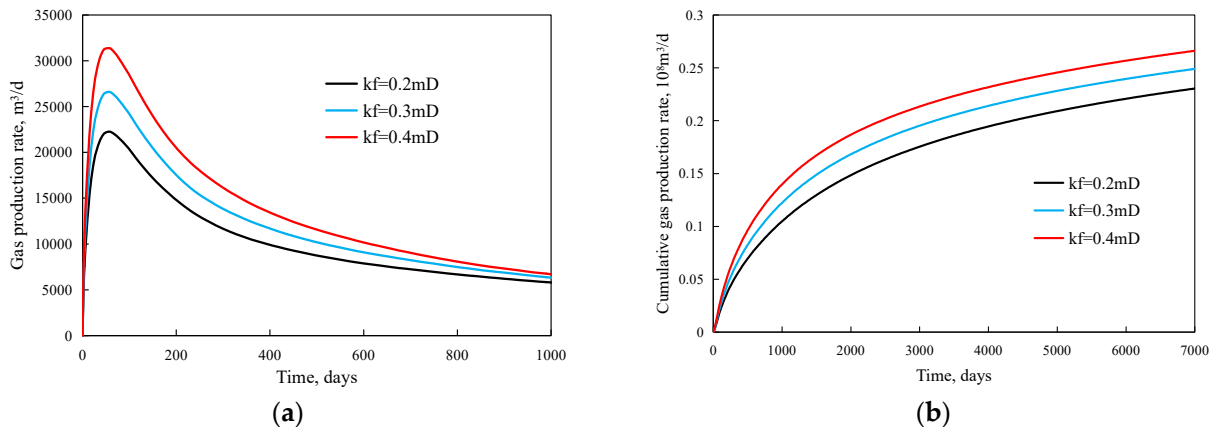


Figure 9. Effect of permeability of the coal cleat in the inner reservoir on gas production rate. (a) Influence of k_f on gas production rate. (b) Influence of k_f on cumulative gas production rate.

Figure 10 presents the effect of the permeability of the coal cleat in the outer reservoir on the gas production capacity of deep CBM wells. The data suggests that higher coal cleat permeability in the outer reservoir significantly influences the initial production capacity. More precisely, as the permeability of the coal cleat in the outer reservoir increases, the time required for the pressure drop to impact the interior of the outer zone matrix decreases, leading to a greater initial production capacity. The underlying reason for this is that higher coal cleat permeability in the outer reservoir allows the pressure drop to more easily impact the exterior of the outer zone matrix, stimulating the desorption of adsorbed gas in the outer zone. However, it is important to note that the permeability of the coal cleat in the

inner reservoir tends to have a more substantial impact on the desorption of gas than the permeability of the coal cleat in the outer reservoir.

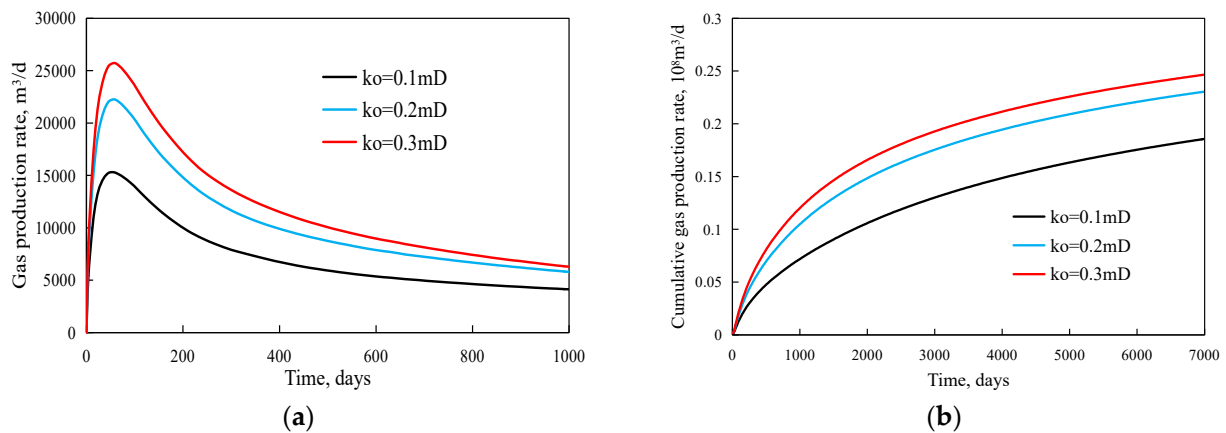


Figure 10. Effect of permeability of the coal cleat in the outer reservoir on gas production rate. (a) Influence of k_o on gas production rate. (b) Influence of k_o on cumulative gas production rate.

Figure 11 demonstrates the influence of the coal cleat's permeability stress sensitivity on the gas productivity of deep CBM wells. As shown in Figure 11, stress sensitivity impacts the entire development lifecycle of the deep CBM reservoir, particularly during the initial and middle stages of production. As the production pressure difference escalates, the permeability loss intensifies, leading to an increase in fluid flow resistance and, ultimately, a reduction in production accompanied by a faster rate of decline. Consequently, judicious management of the production pressure difference for deep CBM reservoirs should be maintained throughout the production process to mitigate the effects of stress sensitivity on production capacity.

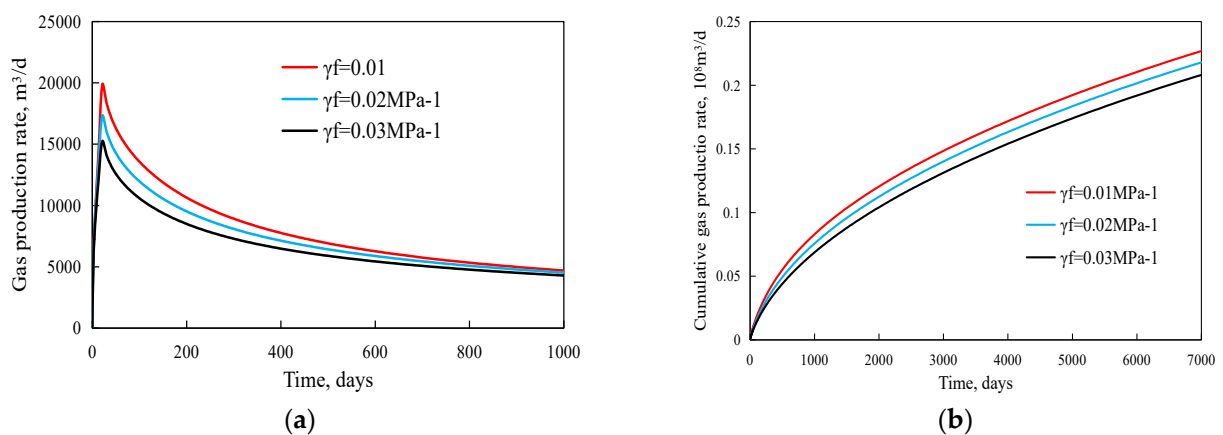


Figure 11. Effect of permeability stress sensitivity of the coal cleat on gas production rate. (a) Influence of γ_f on gas production rate. (b) Influence of γ_f on cumulative gas production rate.

3.3. Field Application

This study employs a deep CBM well situated to demonstrate the effectiveness of the proposed model. The production well is located on the northeast edge of the Ordos Basin, and its tectonic evolution is controlled by the regional tectonic evolution of the Ordos Basin. The burial depth of the main coal seam is controlled by the structure and surface influence, and it is between 1500 m and 2500 m. The burial depth of the coal seam in the southeast direction becomes shallower. The structure in the region is relatively stable, with no development of major faults and more development of inter-layer small faults. The average coal seam thickness is 11 m, the average coal seam Langmuir volume is 15.0 m³/t, and the average coal seam gas content is 14 m³/t. Table 4 details the basic data utilized in

the production data analysis. The selection of parameters in Table 4 is obtained through the actual measurement data report of the example well. From the well logging report, the burial depth of the example well is 2230 m, the coal seam thickness is 13.2 m, and the porosity of the coal cleat is 3%. The pressure gradient of the production well area is 1 MPa/100 m, thus, the initial formation pressure is 22.3 MPa. From the fracturing design report, the number of hydraulic fractures is 14, the length of the horizontal well is 1200 m, and the width of hydraulic fractures is 0.001 m. The initial formation temperature is 320.2 K can be obtained from the well testing report. Moreover, core taking experiment is conducted on the production well, and the parameters of Langmuir pressure, Langmuir volume, and gas content in coal seams are obtained from the gas content report. Production for the well commenced on 1 January 2023. The production dynamic data, spanning from 3 January 2023, to 21 June 2023, were gathered for fitting and interpretation, followed by a prediction of the gas-water two-phase production capacity based on the fitting results.

Table 4. Data used in production data analysis.

Parameters	Symbol	Units	Value
Initial formation pressure	p_i	MPa	22.3
Initial formation temperature	T_i	K	320.2
Bottom-hole pressure	p_{wf}	MPa	4
Formation thickness	h	m	13.2
Number of hydraulic fractures	N_F	Dimensionless	14
Width of hydraulic fractures	w_F	m	0.001
Porosity of hydraulic fractures	Φ_F	Fraction	0.4
Length of the horizontal well	L	m	1200
Half-width of the reservoir	y_e	m	220
Porosity of the coal cleat	Φ_f	Fraction	0.03
Langmuir pressure	p_L	MPa	2.9
Langmuir volume	V_L	m^3/t	13.3
Gas content in coal seams	V	m^3/t	15.7

The proposed medium gas-water two-phase production dynamic prediction method, tailored for deep CBM reservoirs, was employed to fit the production dynamic data of the sample well. Figure 12 illustrates the fitting curves, evidencing a strong fit with the gas-water two-phase production of the deep CBM well. We also show the period with data between 0–200 days in Figure 13. Besides, numerical simulation is also conducted on the basis of production history match. The calculated results with the Eclipse model are compared with the proposed model, which is shown in Figure 13. Because the solution of the proposed model is not limited by the time step, and the fracture and matrix systems do not need to be divided into meshes, the early simulation accuracy is better and the computational efficiency is higher than the Eclipse model. The parameters of the reservoir and fracture, acquired through inversion post-fitting, are listed in Table 5. A comparison between the inversion results, the geological attributes of the original gas reservoir, and actual production outcomes suggest that the key permeability parameters, as identified for the reservoir and fracture, offer theoretical guidance in predicting the production capacity of the CBM well, optimizing the design of fracturing parameters, and evaluating the post-fracturing impacts. Utilizing this model to predict subsequent production, the cumulative gas and water production are projected to be $0.36 \times 10^8 m^3$ and $3.7 \times 10^4 m^3$, respectively. These findings offer valuable insights and guidance in adjusting the development plans for deep CBM reservoirs.

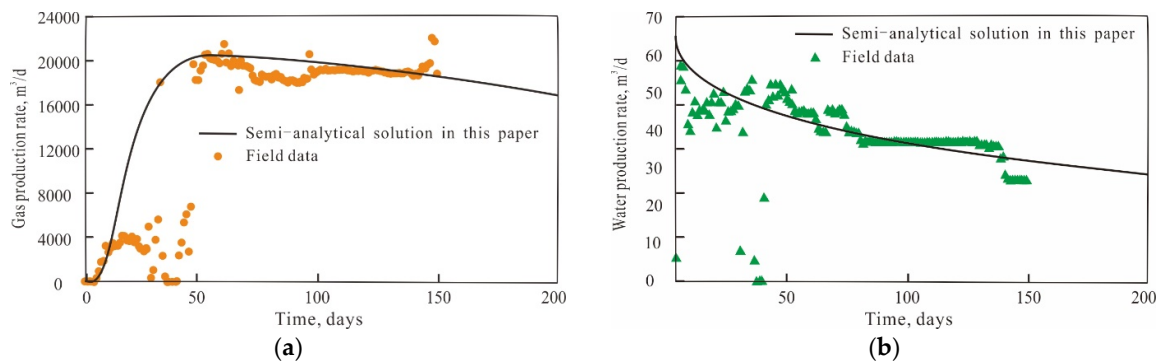


Figure 12. Type curve fitting for the production data with the proposed model. (a) Type curve fitting for the gas production data. (b) Type curve fitting for the water production data.

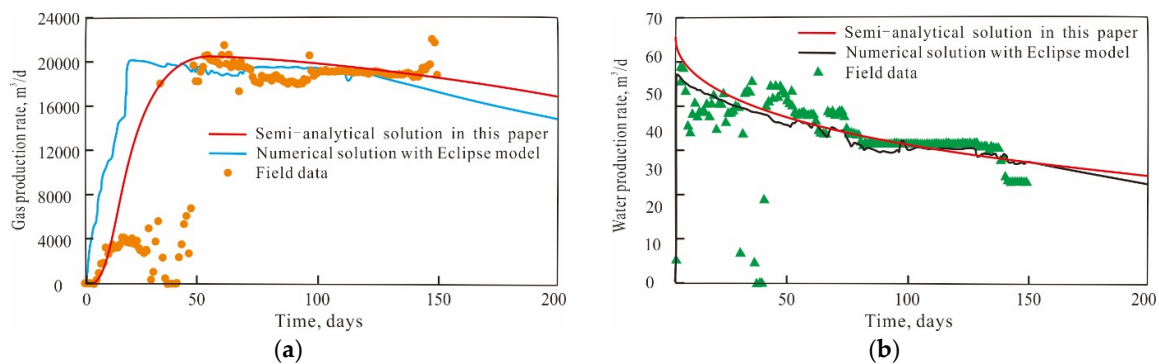


Figure 13. Type curve fitting for the production data with the proposed model and the Eclipse model. (a) Type curve fitting for the gas production data. (b) Type curve fitting for the water production data.

Table 5. Fitting results of the proposed model.

Parameters	Symbol	Units	Value
Conductivity of hydraulic fractures	η_F	mD·m	0.32
Half length of hydraulic fractures	y_F	m	82
Permeability of the coal cleat in the inner reservoir	k_f	mD	0.25
Permeability of the outer reservoir	k_o	mD	0.13
Permeability modulus of the coal cleat	γ_f	MPa ⁻¹	0.05

4. Conclusions

This study introduces a novel methodology for predicting production in deep CBM wells, accounting for intricate fracture characteristics of reservoirs, effects of stress sensitivity, and dual-phase gas-water flow characteristics. The semi-analytical method proposed here, founded on the flowing material balance approach and iterative substitution, effectively addresses gas-water dual-phase non-linear flow issues with appreciable accuracy and computational efficiency. Key conclusions drawn from this study include:

1. Employing the flowing material balance method for computing the average pressure and average saturation of the reservoir, and iteratively updating the non-linear parameters in the seepage model, facilitates the accurate handling of the non-linear seepage problem associated with gas-water dual-phase flow. This results in an efficient and precise resolution of the seepage model;
2. The verification of the numerical model and field applications together suggest that the semi-analytical method investigated in this study offers a high degree of prediction accuracy and can be employed to forecast the production rate of deep CBM wells;
3. Critical seepage parameters of hydraulic fractures significantly influence the production dynamics of gas-water dual-phase. Therefore, hydraulic fracturing should aim

- to enhance the degree and extent of modification to boost the production capacity of deep CBM wells;
4. The stress-sensitive effect of the coal cleats has an impact on the production capacity of deep CBM wells. Therefore, it is necessary to judiciously control the production pressure differential during production to effectively mitigate the adverse influence of stress-sensitive effects.

Author Contributions: Methodology, S.W.; Software, S.W.; Validation, D.L.; Investigation, W.L. All authors have read and agreed to the published version of the manuscript.

Funding: This research was partially funded by CNOOC Research Institute Co., Ltd., Science and Technology Projects (No. CNOOC-YXKJ-QZJC-TJ-2020-01).

Conflicts of Interest: The authors declare no conflict of interest.

References

1. Yang, Z.; Wang, H.; Liu, N.; Li, J. Simulation study of characteristics of hydraulic fracturing propagation of low permeability coal seam. *Disaster Adv.* **2012**, *5*, 717–720.
2. Sun, Z.; Shi, J.; Wu, K.; Zhang, T.; Feng, D.; Li, X. Effect of pressure-propagation behavior on production performance: Implication for advancing low-permeability coalbed-methane recovery. *SPE J.* **2019**, *24*, 681–697. [\[CrossRef\]](#)
3. Chen, Y.; Pan, Z. Reservoir properties of Chinese tectonic coal: A review. *Fuel* **2020**, *260*, 116350. [\[CrossRef\]](#)
4. Ren, J.; Zhang, L.; Ren, S.; Lin, J.; Meng, S.; Ren, G.; Gentzis, T. Multi-branched horizontal wells for coalbed methane production: Field performance and well structure analysis. *Int. J. Coal Geol.* **2014**, *131*, 52–64. [\[CrossRef\]](#)
5. Ma, J.; Chen, J.; Guan, J.; Lin, Y.; Chen, W.; Huang, L. Implementation of Johnson-Holmquist-Beissel model in four-dimensional lattice spring model and its application in projectile penetration. *Int. J. Impact Eng.* **2022**, *170*, 104340. [\[CrossRef\]](#)
6. Ma, J.; Zhao, J.; Lin, Y.; Liang, J.; Chen, J.; Chen, W.; Huang, L. Study on Tamped Spherical Detonation-Induced Dynamic Responses of Rock and PMMA Through Mini-Chemical Explosion Tests and a Four-Dimensional Lattice Spring Model. *Rock Mech. Rock Eng.* **2023**, *56*, 7357–7375. [\[CrossRef\]](#)
7. Wu, X.; Xi, C.; Wang, G. The mathematic model research of complicated fractures system in coalbed methane wells. *Nat. Gas Ind.* **2006**, *26*, 124–126.
8. Pant, L.M.; Huang, H.; Secanell, M.; Larter, S.; Mitra, S.K. Multi scale characterization of coal structure for mass transport. *Fuel* **2015**, *159*, 315–323. [\[CrossRef\]](#)
9. Pan, Z.; Wood, D.A. Coalbed methane (CBM) exploration, reservoir characterisation, production, and modelling: A collection of published research (2009–2015). *J. Nat. Gas Sci. Eng.* **2015**, *26*, 1472–1484. [\[CrossRef\]](#)
10. Zhang, J.; Feng, Q.; Zhang, X.; Hu, Q.; Wen, S.; Chen, D.; Yan, X. Multi-fractured horizontal well for improved coalbed methane production in eastern Ordos basin, China: Field observations and numerical simulations. *J. Pet. Sci. Eng.* **2020**, *194*, 107488. [\[CrossRef\]](#)
11. Yang, Y.; Liu, S. Integrated modeling of multi-scale transport in coal and its application for coalbed methane recovery. *Fuel* **2021**, *300*, 120971. [\[CrossRef\]](#)
12. Sun, Z.; Huang, B.; Li, Y.; Yu, W.; Ji, L. Production forecast of fractured vertical wells in coalbed methane reservoirs: Coupling dynamic drainage area. *Arab. J. Geosci.* **2022**, *15*, 7. [\[CrossRef\]](#)
13. Shi, X.; Pan, J.; Hou, Q.; Jin, Y.; Wang, Z.; Niu, Q.; Li, M. Micrometer-scale fractures in coal related to coal rank based on micro-CT scanning and fractal theory. *Fuel* **2018**, *212*, 162–172. [\[CrossRef\]](#)
14. Zhang, T.; Zhang, L.; Zhao, Y.; Zhang, R.; Zhang, D.; He, X.; Ge, F.; Wu, J.; Javadpour, F. Ganglia dynamics during imbibition and drainage processes in nanoporous systems. *Phys Fluids.* **2022**, *34*, 042016. [\[CrossRef\]](#)
15. Zhang, T.; Luo, S.; Zhou, H.; Hu, H.; Zhang, L.; Zhao, Y.; Javadpour, F. Pore-scale modelling of water sorption in nanopore systems of shale. *Int. J. Coal Geol.* **2023**, *27*, 104266. [\[CrossRef\]](#)
16. Clarkson, C.R.; Qanbari, F. Transient flow analysis and partial water relative permeability curve derivation for low permeability undersaturated coalbed methane wells. *Int. J. Coal Geol.* **2015**, *152*, 110–124. [\[CrossRef\]](#)
17. Zhao, J.; Tang, D.; Lin, W.; Xu, H.; Li, Y.; Tao, S.; Lv, Y. Permeability dynamic variation under the action of stress in the medium and high rank coal reservoir. *J. Nat. Gas Sci. Eng.* **2015**, *26*, 1030–1041. [\[CrossRef\]](#)
18. Tang, X.; Wang, Z.; Ripepi, N.; Kang, B.; Yue, G. Adsorption affinity of different types of coal: Mean isosteric heat of adsorption. *Energy Fuels* **2015**, *29*, 3609–3615. [\[CrossRef\]](#)
19. Zeng, Q.; Wang, Z. Stress and temperature sensitivity of coal permeability in the Eastern Ordos Basin. *Pet. Sci. Bull.* **2020**, *4*, 512–519.
20. Yu, P.; Dempsey, D.; Archer, R. Techno-Economic feasibility of enhanced geothermal systems (EGS) with partially bridging multi-stage fractures for district heating applications. *Energy Convers. Manag.* **2022**, *257*, 115405. [\[CrossRef\]](#)
21. Aminian, K.; Ameri, S. Predicting production performance of CBM reservoirs. *J. Nat. Gas Sci. Eng.* **2009**, *1*, 25–30. [\[CrossRef\]](#)

22. Salmachi, A.; Yarmohammadtooski, Z. Production data analysis of coalbed methane wells to estimate the time required to reach to peak of gas production. *Int. J. Coal Geol.* **2015**, *141*, 33–41. [[CrossRef](#)]
23. Yan, X.; Zhang, S.; Tang, S.; Li, Z.; Guan, W.; Zhang, Q.; Wang, J. A prediction model for pressure propagation and production boundary during coalbed methane development. *Energy Fuels* **2021**, *35*, 1219–1233. [[CrossRef](#)]
24. Shi, J.; Jia, Y.; Wu, J.; Xu, F.; Sun, Z.; Liu, C.; Liu, C. Dynamic performance prediction of coalbed methane wells under the control of bottom-hole pressure and casing pressure. *J. Pet. Sci. Eng.* **2021**, *196*, 107799. [[CrossRef](#)]
25. Yu, P.; Dempsey, D.; Rinaldi, A.P.; Calibugan, A.; Ritz, V.A.; Archer, R. Association between Injection and Microseismicity in Geothermal Fields with Multiple Wells: Data-driven Modelling of Rotokawa, New Zealand, and Húsmúli, Iceland. *J. Geophys. Res. Solid Earth* **2022**, *128*, e2022JB025952. [[CrossRef](#)]
26. Ibrahim, A.F.; Nasr-El-Din, H.A. A comprehensive model to history match and predict gas/water production from coal seams. *Int. J. Coal Geol.* **2015**, *146*, 79–90. [[CrossRef](#)]
27. Ma, T.; Rutqvist, J.; Oldenburg, C.M.; Liu, W.; Chen, J. Fully coupled two-phase flow and poromechanics modeling of coalbed methane recovery: Impact of geomechanics on production rate. *J. Nat. Gas Sci. Eng.* **2017**, *45*, 474–486. [[CrossRef](#)]
28. Sun, Z.; Shi, J.; Zhang, T.; Wu, K.; Feng, D.; Sun, F.; Li, X. A fully-coupled semi-analytical model for effective gas/water phase permeability during coal-bed methane production. *Fuel* **2018**, *223*, 44–52. [[CrossRef](#)]
29. Shi, J.; Hou, C.; Wang, S.; Xiong, X.; Wu, S.; Liu, C. The semi-analytical productivity equations for vertically fractured coalbed methane wells considering pressure propagation process, variable mass flow, and fracture conductivity decrease. *J. Pet. Sci. Eng.* **2019**, *178*, 528–543. [[CrossRef](#)]
30. Zou, M.; Wei, S.; Huang, Z.; Lv, X.; Guo, B. Simulations on recoverability performances for a coalbed methane field in SE edge of Ordos basin, China. *Fuel* **2018**, *233*, 354–360. [[CrossRef](#)]
31. Zhu, S.; Salmachi, A.; Du, Z. Two phase rate-transient analysis of a hydraulically fractured coal seam gas well: A case study from the Ordos Basin, China. *Int. J. Coal Geol.* **2018**, *195*, 47–60. [[CrossRef](#)]
32. Peng, X.; Zhu, S.; You, Z.; Du, Z.; Deng, P.; Wang, C.; Wang, M. Numerical simulation study of fines migration impacts on an early water drainage period in undersaturated coal seam gas reservoirs. *Geofluids* **2019**, *2019*, 5723694. [[CrossRef](#)]
33. Yu, P.; Dempsey, D.; Archer, R. A three-dimensional coupled thermo-hydro-mechanical numerical model with partially bridging multi-stage contact fractures in horizontal-well enhanced geothermal system. *Int. J. Rock Mech. Min. Sci.* **2021**, *143*, 104787. [[CrossRef](#)]
34. Sun, Z.; Huang, B.; Liu, Y.; Jiang, Y.; Zhang, Z.; Hou, M.; Li, Y. Gas-phase production equation for CBM reservoirs: Interaction between hydraulic fracturing and coal orthotropic feature. *J. Pet. Sci. Eng.* **2022**, *213*, 110428. [[CrossRef](#)]
35. Song, P.; Li, Y.; Yin, Z.; Yuan, Q. Hydrogen generation from heavy oils via in-situ combustion gasification. In *SPE Western Regional Meeting*; SPE: Kuala Lumpur, Malaysia, 2023; p. D031S007R003.
36. Nossent, J.; Elsen, P.; Bauwens, W. Sobol' sensitivity analysis of a complex environmental model. *Environ. Model. Softw.* **2011**, *26*, 1515–1525. [[CrossRef](#)]
37. Yin, Z.; Feng, T.; MacBeth, C. Fast assimilation of frequently acquired 4D seismic data for reservoir history matching. *Comput. Geosci.* **2019**, *128*, 30–40. [[CrossRef](#)]
38. Clarkson, C.R.; Qanbari, F. A semi-analytical forecasting method for unconventional gas and light oil wells: A hybrid approach for addressing the limitations of existing empirical and analytical methods. *SPE Reserv. Eval. Eng.* **2014**, *18*, 260–263.

Disclaimer/Publisher's Note: The statements, opinions and data contained in all publications are solely those of the individual author(s) and contributor(s) and not of MDPI and/or the editor(s). MDPI and/or the editor(s) disclaim responsibility for any injury to people or property resulting from any ideas, methods, instructions or products referred to in the content.